Experimental demonstration of titanium nitride plasmonic interconnects

N. Kinsey,[1] M. Ferrera,[1,2] G. V. Naik,[1,3] V. E. Babicheva,[4] V. M. Shalaev,[1] and A. Boltasseva[1,4,*]

[1]*School of Electrical & Computer Engineering and Birck Nanotechnology Center, Purdue University, 1205 West State Street, West Lafayette, Indiana 47907-2057, USA*

[2]*Also with the School of Engineering and Physical Sciences, Heriot-Watt University, David Brewster Building, Edinburgh, Scotland EH14 4AS, UK*

[3]*School of Materials Science and Engineering, Stanford University, Durand Building, 496 Lomita Mall, Stanford, California 94305-4034, USA*

[4]*DTU Fotonik – Department of Photonics Engineering, Technical University of Denmark, Oersteds Plads 343, DK-2800 Kgs. Lyngby, Denmark*

**aeb@purdue.edu*

Abstract: An insulator-metal-insulator plasmonic interconnect using TiN, a CMOS-compatible material, is proposed and investigated experimentally at the telecommunication wavelength of 1.55 μm. The TiN waveguide was shown to obtain propagation losses less than 0.8 dB/mm with a mode size of 9.8 μm on sapphire, which agree well with theoretical predictions. A theoretical analysis of a solid-state structure using Si_3N_4 superstrates and ultra-thin metal strips shows that propagation losses less than 0.3 dB/mm with a mode size of 9 μm are attainable. This work illustrates the potential of TiN as a realistic plasmonic material for practical solid-state, integrated nano-optic and hybrid photonic devices.

OCIS codes: (250.5403) Plasmonics; (240.6680) Surface plasmons; (230.7370) Waveguides; (200.4650) Optical interconnects; (160.3130) Integrated optics materials.

References and links

1. R. Soref, "The past, present, and future of silicon photonics," IEEE J. Sel. Top. Quantum Electron. **12**(6), 1678–1687 (2006).
2. S. Assefa, S. Shank, W. Green, M. Khater, E. Kiewra, C. Reinholm, S. Kamlapurkar, C. Schow, F. Horst, H. Pan, T. Topuria, P. Rice, D. M. Gill, J. Rosenberg, and T. Barwicz, "A 90nm CMOS integrated nano-photonics technology for 25Gbps WDM optical communications applications," in *IEEE International Electron Devices Meeting* (San Francisco, CA, 2012).
3. Intel Corporation, "Thunderbolt Technology," in *Technology Brief* (2012).
4. D. K. Gramotnev and S. I. Bozhevolnyi, "Plasmonics beyond the diffraction limit," Nat. Photonics **4**(2), 83–91 (2010).
5. P. Berini, "Long-range surface plasmon polaritons," Adv. Opt. Photon. **1**(3), 484 (2009).
6. A. Kumar, J. Gosciniak, V. S. Volkov, S. Papaioannou, D. Kalavrouziotis, K. Vyrsokinos, J. Weeber, K. Hassan, L. Markey, A. Dereux, T. Tekin, M. Waldow, D. Apostolopoulos, H. Avramopoulos, N. Pleros, and S. I. Bozhevolnyi, "Dielectric-loaded plasmonic waveguide components: Going practical," Laser Photon. Rev. **7**(6), 1–14 (2013).
7. H. Cho, S. Member, P. Kapur, and K. C. Saraswat, "Power Comparison between high-speed electrical and optical interconnects for interchip communication," IEEE J. Lightw. Technol. **22**(9), 2021–2033 (2004).
8. H. M. G. Wassel, S. Member, D. Dai, M. Tiwari, J. K. Valamehr, L. Theogarajan, J. Dionne, F. T. Chong, and T. Sherwood, "Opportunities and Challenges of Using Plasmonic Components in Nanophotonic Architectures," IEEE J. Emerg. Sel. Topics Circuits Syst. **2**(2), 154–168 (2012).
9. M. Kobrinsky, B. Block, J. Zheng, B. Barnett, E. Mohammed, M. Reshotko, F. Robertson, S. List, I. Young, and K. Cadien, "On-Chip Optical Interconnects," Intel Technol. J. **8**(2), 129–142 (2004).
10. V. E. Babicheva, N. Kinsey, G. V. Naik, M. Ferrera, A. V. Lavrinenko, V. M. Shalaev, and A. Boltasseva, "Towards CMOS-compatible nanophotonics: ultra-compact modulators using alternative plasmonic materials," Opt. Express **21**(22), 27326–27337 (2013).
11. R. Charbonneau, P. Berini, E. Berolo, and E. Lisicka-Shrzek, "Experimental observation of plasmon polariton waves supported by a thin metal film of finite width," Opt. Lett. **25**(11), 844–846 (2000).

#207666 - $15.00 USD Received 4 Mar 2014; revised 16 Apr 2014; accepted 6 May 2014; published 13 May 2014

12. T. Nikolajsen, K. Leosson, I. Salakhutdinov, and S. I. Bozhevolnyi, "Polymer-based surface-plasmon-polariton stripe waveguides at telecommunication wavelengths," Appl. Phys. Lett. **82**(5), 668 (2003).
13. A. Boltasseva, T. Nikolajsen, K. Leosson, K. Kjaer, M. S. Larsen, and S. I. Bozhevolnyi, "Integrated optical components utilizing long-range surface plasmon polaritons," IEEE J. Lightw. Technol. **23**(1), 413–422 (2005).
14. P. Berini, R. Charbonneau, N. Lahoud, and G. Mattiussi, "Characterization of long-range surface-plasmon-polariton waveguides," J. Appl. Opt. **98**(4), 043109 (2005).
15. J. Kim, S. Park, J. Ju, S. K. Park, M. Kim, and M. Lee, "Low-loss polymer-based long-range surface plasmon-polariton waveguide," IEEE Photon. Technol. Lett. **19**(18), 1374–1376 (2007).
16. J. Jiang, C. L. Callender, S. Jacob, J. P. Noad, S. Chen, J. Ballato, and D. W. Smith, Jr., "Long-range surface plasmon polariton waveguides embedded in fluorinated polymer," Appl. Opt. **47**(21), 3892–3900 (2008).
17. S. Park, J. J. Ju, J. T. Kim, M. S. Kim, S. K. Park, J. M. Lee, W. J. Lee, and M. H. Lee, "Sub-dB/cm propagation loss in silver stripe waveguides," Opt. Express **17**(2), 697–702 (2009).
18. V. J. Sorger, N. D. Lanzillotti-Kimura, R. Ma, and X. Zhang, "Ultra-compact silicon nanophotonic modulator with broadband response," Nanophoton. **1**(1), 17–22 (2012).
19. J. A. Dionne, K. Diest, L. A. Sweatlock, and H. A. Atwater, "PlasMOStor: a metal-oxide-Si field effect plasmonic modulator," Nano Lett. **9**(2), 897–902 (2009).
20. Z. Lu, W. Zhao, and K. Shi, "Ultracompact electroabsorption modulators based on tunable epsilon-near-zero-slot waveguides," IEEE Photon. J. **4**(3), 735–740 (2012).
21. A. Falk, F. Koppens, C. Yu, K. Kang, N. Snapp, A. Akimov, M. Jo, M. Lukin, and H. Park, "Near-field electrical detection of optical plasmons and single-plasmon sources," Nat. Phys. **5**(7), 475–479 (2009).
22. O. Krupin, H. Asiri, C. Wang, R. N. Tait, and P. Berini, "Biosensing using straight long-range surface plasmon waveguides," Opt. Express **21**(1), 698–709 (2013).
23. A. Kumar, J. Gosciniak, T. B. Andersen, L. Markey, A. Dereux, and S. I. Bozhevolnyi, "Power monitoring in dielectric-loaded surface plasmon-polariton waveguides," Opt. Express **19**(4), 2972–2978 (2011).
24. P. Berini, "Figures of merit for surface plasmon waveguides," Opt. Express **14**(26), 13030–13042 (2006).
25. G. V. Naik, J. L. Schroeder, X. Ni, A. V. Kildishev, T. D. Sands, and A. Boltasseva, "Titanium nitride as a plasmonic material for visible and near-infrared wavelengths," Opt. Mater. Express **2**(4), 478–489 (2012).
26. G. V. Naik, V. M. Shalaev, and A. Boltasseva, "Alternative plasmonic materials: beyond gold and silver," Adv. Mater. **25**(24), 3264–3294 (2013).
27. D. Steinmuller-Nethl, R. Kovacs, E. Gornik, and P. Rodhammer, "Excitation of surface plasmons on titanium nitride films: determination of the dielectric function," Thin Solid Films **237**(1), 277–281 (1994).
28. M. B. Cortie, J. Giddings, and A. Dowd, "Optical properties and plasmon resonances of titanium nitride nanostructures," Nanotechnology **21**(11), 115201 (2010).
29. A. Hibbins, J. Sambles, and C. Lawrence, "Surface plasmon-polariton study of the optical dielectric function of titanium nitride," J. Mod. Opt. **45**(10), 2051–2062 (1998).
30. N. Chen, W. Lien, C. Liu, Y. Huang, Y. Lin, C. Chou, S. Chang, and C. Ho, "Excitation of surface plasma wave at TiN/air interface in the Kretschmann geometry," J. Appl. Opt. **109**(4), 043104 (2011).
31. A. Emboras, R. M. Briggs, A. Najar, S. Nambiar, C. Delacour, P. Grosse, E. Augendre, J. M. Fedeli, B. de Salvo, H. A. Atwater, and R. Espiau de Lamaestre, "Efficient coupler between silicon photonic and metal-insulator-silicon-metal plasmonic waveguides," Appl. Phys. Lett. **101**(25), 251117 (2012).
32. C. Delacour, S. Blaize, P. Grosse, J. M. Fedeli, A. Bruyant, R. Salas-Montiel, G. Lerondel, and A. Chelnokov, "Efficient directional coupling between silicon and copper plasmonic nanoslot waveguides: toward metal-oxide-silicon nanophotonics," Nano Lett. **10**(8), 2922–2926 (2010).
33. K. MacDonald, Z. Sámson, M. Stockman, and N. Zheludev, "Ultrafast active plasmonics," Nat. Photonics **3**(1), 55–58 (2009).
34. A. Emboras, A. Najar, S. Nambiar, P. Grosse, E. Augendre, C. Leroux, B. de Salvo, and R. E. de Lamaestre, "MNOS stack for reliable, low optical loss, Cu based CMOS plasmonic devices," Opt. Express **20**(13), 13612–13621 (2012).
35. S. Zhu, G. Q. Lo, and D. L. Kwong, "Components for silicon plasmonic nanocircuits on horizontal Cu-SiO_2-Si-SiO_2-Cu nanoplasmonic waveguides," Opt. Express **20**(6), 5867–5881 (2012).
36. S. Zhu, G. Q. Lo, and D. L. Kwong, "Electro-absorption modulation in horizontal metal-insulator-silicon-insulator-metal nanoplasmonic slot waveguides," Appl. Phys. Lett. **99**(15), 151114 (2011).
37. X. Shi, X. Zhang, Z. Han, U. Levy, and S. I. Bozhevolnyi, "CMOS-compatible long-range dielectric-loaded plasmonic waveguides," IEEE J. Lightw. Technol. **31**(21), 3361–3367 (2013).
38. S. Kurtz and R. Hordon, "Chemical vapor deposition of titanium nitride at low temperatures," Thin Solid Films **140**(2), 277–290 (1986).
39. S. Heil, E. Langereis, F. Roozeboom, M. Sanden, and W. Kessels, "Low-temperature deposition of TiN by plasma-assisted atomic layer deposition," J. Electrochem. Soc. **153**(11), G956–G965 (2006).
40. R. Geffken and S. Luce, "Method of forming a self-aligned copper diffusion barrier in vias," US Patent 5,985,762 (1999).
41. S. I. Bozhevolnyi, *Plasmonic Nanoguides and Circuits* (Stanford Publishing, 2008).
42. S. A. Maier, *Plasmonics: Fundamentals and Applications* (2007).
43. G. I. Stegeman, R. F. Wallis, and A. A. Maradudin, "Excitation of surface polaritons by end-fire coupling," Opt. Lett. **8**(7), 386–388 (1983).

#207666 - $15.00 USD Received 4 Mar 2014; revised 16 Apr 2014; accepted 6 May 2014; published 13 May 2014

44. C. D. Sheraw, D. J. Gundlach, and R. N. Jackson, "Spin-on polymer gate dielectric for high performance organic thin film transistors," MRS Proceedings **583** (1999).
45. V. S. Volkov, Z. Han, M. G. Nielsen, K. Leosson, H. Keshmiri, J. Gosciniak, O. Albrektsen, and S. I. Bozhevolnyi, "Long-range dielectric-loaded surface plasmon polariton waveguides operating at telecommunication wavelengths," Opt. Lett. **36**(21), 4278–4280 (2011).
46. R. F. Oulton, V. J. Sorger, D. a. Genov, D. F. P. Pile, and X. Zhang, "A hybrid plasmonic waveguide for subwavelength confinement and long-range propagation," Nature Photon. **2,** 496–500 (2008).

1. Introduction

Integrated optical technologies offer unprecedented bandwidth, propagation loss, and noise reduction - advantages that are harnessed in current telecommunication networks and a limited number of commercial devices [1–3]. However, a limiting factor which has prevented ubiquitous adoption of integrated optical components is the restriction on the minimum size of components due to the diffraction limited nature of light. As a potential solution to the disparity between the size scales of photonics and electronics, plasmonics presents the ability to tightly confine and guide light at the nanoscale by coupling with the momentum of free electrons at a metal-dielectric interface, called surface plasmon polaritons (SPPs) (see reviews of waveguide structures [4–6]).

While the introduction of the metallic layer allows for the nanoscale confinement of light, it also introduces significant and unavoidable ohmic losses in the structure. Generally, losses associated with transmission and generation of light/SPPs consumes equivalent if not more power than electrical devices [7–9]. However, as the operational frequency of these devices increases, especially closer to that available with optical devices, the power consumption in electrical interconnects would be significantly larger than with optical interconnects [7]. Additionally, ohmic losses may be affordable, and desired, for specific nano-photonic applications (i.e. modulators) which may still possess a high figure of merit despite the larger magnitude of the propagation loss [10]. Other structures, such as interconnects, are less tolerable of propagation losses and many efforts have been taken to reduce this loss. Specifically, research into the long range surface plasmon polariton (LR-SPP) mode allowed the propagation loss of devices to progress quite rapidly, with several devices now demonstrating losses on the order of integrated photonic waveguides [11–17]. Although these devices tend to have a larger mode size than photonic waveguides, using a plasmonic interconnect structure enables numerous important technological advantages which may offset the lack of modal confinement.

Plasmonic interconnects retain many of the important benefits of photonic interconnects such as reduced cross-talk, low signal delay time, and high bandwidth, but have several additional advantages such as an inherent ability to couple with active plasmonic structures, an extreme sensitivity to the metallic-dielectric interface, and support for both optical and electrical signals. Extremely compact active plasmonic devices, such as plasmonic modulators, switches, detectors, and sensors, can achieve high performance when using tightly confined SPP modes [10, 18–21]. However, coupling into these devices from low-loss interconnect structures can be difficult. Unlike photonics, plasmonic interconnect structures possess an inherent ability to couple with these devices with reduced coupling losses. Also, the extreme sensitivity of the SPP to the metal-dielectric interface is key for many applications such as sensors, modulators, and couplers. Small perforations or index changes at the interface can result in drastic changes to the SPPs properties allowing for a host of active devices [22]. Finally, the metallic nature of the plasmonic waveguide allows it to carry both optical and electrical signals [23]. This is particularly important for electro-optic chips and devices where a plasmonic waveguide could carry both DC power, or act as a ground contact for an in-line SPP filter or modulator, while carrying a high speed data stream of plasmons. This can greatly reduce the complexity of highly integrated circuit designs and save valuable space on the chip. These advantages, along with comparable performance, make plasmonic

#207666 - $15.00 USD Received 4 Mar 2014; revised 16 Apr 2014; accepted 6 May 2014; published 13 May 2014

waveguides more technologically compatible with next generation integrated nano-optic devices than photonic waveguides.

While many novel plasmonic waveguide structures and devices have been demonstrated with exceptional performance and features, these structures have primarily used noble metals. Such materials provide some of the highest figures of merit, but they are not compatible with the CMOS process [24]. Therefore, to fully harness the advantages of integrated plasmonic devices, the next step is to produce structures which use alternative CMOS-compatible materials, while achieving performance levels that are comparable to both photonic waveguides and other noble-metal-based plasmonic waveguides.

The push for alternative plasmonic materials has led to several platforms which obtain enhanced functionality and performance over many spectral ranges [25, 26]. In the near infrared (NIR) region, the metal-nitride family (ZrN, HfN, TaN, TiN, and others) has been suggested as an important class of materials for plasmonic waveguiding applications. Additionally, the metallic-nitrides have several technological advantages such as tunable optical properties, high thermal stability, chemical stability, mechanical toughness, epitaxial growth on MgO, c-sapphire and silicon, and bio-compatibility. Among these, TiN has received increased attention due to its gold-like optical properties and CMOS-compatibility. Because of this, TiN is an attractive material for many applications, including plasmonics, where its performance has been previously studied using gratings and prism coupling to excite SPPs [25, 27–30].

In this paper we investigate low-loss plasmonic strip waveguides at the telecommunication wavelength of 1.55 μm which utilize the CMOS-compatible plasmonic material TiN. TiN is chosen over other CMOS-compatible plasmonic materials, such as copper and aluminum from which successful devices have been demonstrated, due to its technological advantages [31–37]. A discussion on TiN and its advantages will be presented in the following section, along with fabrication and experimental considerations. Results of modal analysis and cut-back loss measurements on the structure will be presented in Section 3, along with a short discussion. In Section 4, a solid-state version of the waveguide which utilizes a silicon nitride (Si_3N_4) superstrate will be theoretically investigated.

2. Materials and methods

The TiN films used in this work were deposited on c-sapphire using DC reactive magnetron sputtering at 800°C in an argon/nitrogen environment. To obtain full CMOS-compatibility for the TiN film, two problems remain: the deposition temperature and method. However, the previous two points can, in principle, be addressed simultaneously by using alternative deposition techniques such as chemical vapor deposition and atomic layer deposition. These methods have been optimized to produce good electrical quality TiN films at low temperatures (i.e. CMOS-compatible) [38, 39]. Now that the attention has shifted towards the optical properties, there is no reason to believe that these methods cannot also be optimized to produce TiN with the desired optical properties. Also, the use of other CMOS-compatible plasmonic materials, such as copper and aluminum, require a thin layer of TiN to prevent diffusion into silicon [40]. Additionally, these materials oxidize at room temperature, which degrades their optical properties. Therefore, it would be highly beneficial for CMOS-compatible TiN films to be used for plasmonic applications without the need for an additional copper or aluminum layer.

The strip waveguide geometry has been considered for its ability to support the LR-SPP mode, and minimize the propagation losses in the interconnect [13]. In this configuration, the minimum propagation loss is associated with an energy distribution that is symmetric in the direction normal to the interface, requiring an index match between the substrate and superstrate, see schematic in Fig. 1(a) [41, 42]. Index matching oil was used to obtain this condition. The width of the TiN strip was 9.38 μm, see Fig. 1(b), chosen to obtain maximum mode overlap with standard single mode polarization maintaining fiber, and the thickness was

#207666 - $15.00 USD Received 4 Mar 2014; revised 16 Apr 2014; accepted 6 May 2014; published 13 May 2014

chosen to be 10 nm. These dimensions also provide nearly identical operating conditions as previously reported strip waveguides based on gold, allowing for a fair performance comparison between the materials [13]. The width was verified using SEM analysis, with a negligible error bar, and the thickness was determined from the cross section TEM and spectroscopic ellipsometry fitting with an error bar of ± 1 nm, see Fig. 1(c). The TEM illustrates the epitaxial nature of the TiN film on c-sapphire (grows in <111> orientation), as its cubic structure is evident. Such high quality films are paramount for minimizing the losses in plasmonic waveguide structures.

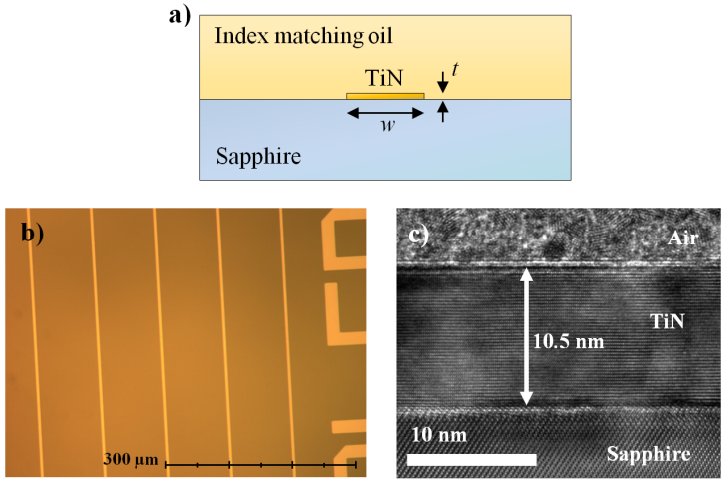

Fig. 1. a) Schematic view of the waveguide geometry cross-section. This illustrates the critical dimension parameters of the strip. b) Optical microscope image of the TiN waveguides fabricated on sapphire. c) Cross-section TEM of the TiN layer on sapphire used for verifying the thickness of the film. This was fed into the ellipsometry measurements to reduce parameter coupling during the extraction of optical properties. The epitaxial-quality of the TiN film can be seen as its cubic lattice structure is evident.

The waveguides were fabricated using a lift-off technique. First, a sacrificial layer of chrome was deposited and AZ1518 photoresist was spin coated on top. The resist was exposed and developed using standard photolithography and the pattern was transferred to the chrome using a chlorine-based reactive ion etch. The thin TiN layer was then deposited onto the sample and the chrome layer was removed using the CR-14S chrome etchant. In preparation for testing, the sample was then cleaved perpendicular to the direction of the waveguides to maximize the coupling efficiency.

The permittivity of the TiN used in this work is $\varepsilon_{TiN} = -75 + 23i$ at 1.55 µm, obtained from spectroscopic ellipsometry. Sapphire (n = 1.75 at 1.55 µm) is used as a substrate due to the high quality, ultra-thin (~2 nm) TiN films which can be deposited along with the availability of index matching oils (Cargille products M-x/1815Y, n = 1.7500 ± 0.0005 at 1.55 µm). Additionally, higher index materials, such as silicon, tightly confine the SPP mode, causing an increased interaction with the metal and larger propagation losses when compared to lower index substrates and claddings. Therefore, for this initial study, sapphire was used to minimize the propagation losses. However, experimental results show that plasmonic TiN can be grown on other substrates such as glass ($\varepsilon_{TiN} = -72 + 22i$) or silicon ($\varepsilon_{TiN} = -46 + 26i$) with good optical properties.

The waveguide was excited using the standard end-fire technique [43]. A 1.55 µm source (Agilent technologies 8164A) was coupled into a single mode polarization maintaining fiber, passed through a polarization controller, and then coupled into the waveguide. The polarization controller allowed for the notable plasmonic TM-TE dependence to be observed, since plasmons can only be excited with a TM polarization. The output of the waveguide was

#207666 - $15.00 USD Received 4 Mar 2014; revised 16 Apr 2014; accepted 6 May 2014; published 13 May 2014

captured by an InGaAs array (Xenics XEVA-1.7-320) with variable 5x – 120x zoom configured in the end-fire detection scheme, which was also calibrated to act as a power meter. This allowed for both a modal analysis of the waveguide as well as a loss-measurement by the cut-back method.

3. Experimental results and discussion

In addition to characterizing the TiN waveguides, it is also important to compare their performance to other similar structures. To do so we use two figures of merit (FoMs). The first is a standard figure of merit considering only the material properties of the plasmonic structure, given in Eq. (1) [41, 42]. The second was adopted from a 1-D FoM proposed by P. Berini but was modified to account for different refractive indices, given in Eq. (2) [24]. We note here that a 1-D approximation of the 2-D structure is a reasonable assumption when the strip width is large [41]. The second figure of merit is considered because it relies on the experimentally measured performance of the structure, thereby including not only the material parameters but also the structure's quality.

$$FoM_1 = \frac{\mathrm{Re}\{\varepsilon\}}{\mathrm{Im}\{\varepsilon\}} \tag{1}$$

$$FoM_2 = \frac{L_{prop}}{n\delta_z} \tag{2}$$

In the FoMs, ε is the metal permittivity, L_{prop} is the propagation length (defined as the 1/e decay of the power), n is the cladding refractive index, and δ_z is the mode size ($1/e^2$ decay of the power) in the vertical direction.

The first step to characterize the TiN waveguide was to perform a modal analysis. An image of the observed mode, along with a vertical intensity profile is shown in Fig. 2(a) and 2(b). Upon fitting this intensity profile with the characteristic exponential decay of the plasmonic mode ($y = c\exp(bz)$ was fit for both sides of the measured data), a good agreement was found except for the portion of the mode near the metal. The peak in the exponential function cannot be accurately captured in the far-field due to the conversion of the plasmonic mode into a propagating photonic mode. Similar situations have been encountered in previous works [13]. Due to this, points greater than 0.8 were excluded from the fitting of the experimental results. There is also a slight asymmetry in the modal cutline resulting from a small mismatch between the refractive indices of the sapphire and index matching oil on the order of 10^{-3}.

The mode size of the TiN waveguide (defined as the $1/e^2$ decay of the power in the z-direction of the fitted curves) was found to be 9.8 μm. However, the sloped nature of the index matching oil as it approaches the waveguide output introduces aberrations in the image, and the actual mode size is expected to be slightly smaller. By using a solid-state superstrate, potentially Si_3N_4, to obtain an effective index match, the lensing effect can be eliminated to provide a cleaner modal measurement. This situation will be theoretically investigated in the following section. Despite this, the mode size observed for the TiN structure is much smaller than similar gold waveguides (δ_z ~20 μm) [13]. This is mainly due to the fact that TiN has a smaller real part of the permittivity, resulting in tighter confinement of the field (field penetrates more into TiN compared to gold) as well as the different refractive indices used for claddings.

An eigenmode simulation on this geometry using the commercial software COMSOL Multiphysics® was completed to compare with the experimental results. The results of the simulation and subsequent curve fitting are shown in Fig. 2(c) and 2(d), obtaining a mode size of 8.0 μm. Evaluation of this simulation confirms that the observed mode size is larger than expected.

#207666 - $15.00 USD Received 4 Mar 2014; revised 16 Apr 2014; accepted 6 May 2014; published 13 May 2014

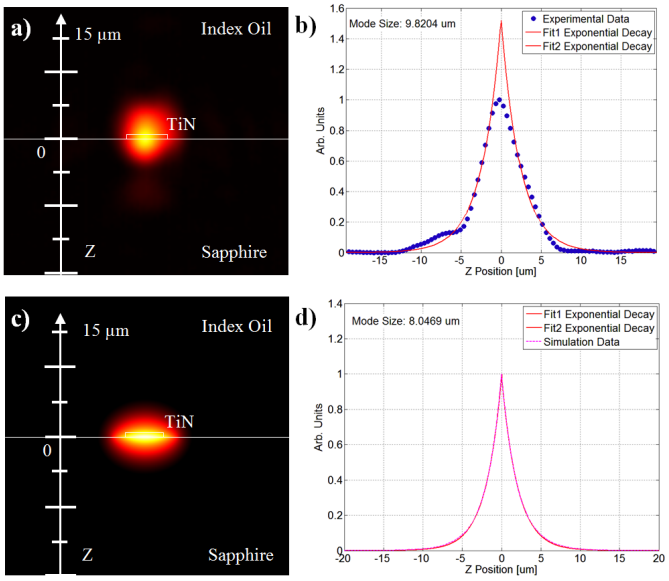

Fig. 2. a) Experimentally measured modal profile from the output facet of the TiN strip waveguide. b) Fitting of the z-cutline intensity with the typical exponential decay of the plasmonic mode. c) Simulated modal profile from COMSOL Multiphysics®. d) Fitting of the z-cutline with exponential decay functions. The fit was $y = c\ \exp(bz)$. Each side of the exponential was fit separately and stitched together for observation. Both show a root mean square error less than 0.02. Note the thickness of the TiN strip is enlarged for reference.

To perform a loss-measurement on the waveguide structure, the NIR camera was calibrated to act as a relative power meter. This was accomplished by measuring the total pixel intensity captured within a fixed pixel area for fixed camera and excitation conditions. As such, the only variables with can affect the measured output intensity are coupling conditions and fabrication irregularities. These factors were mitigated through careful fiber alignment and averaging of the measurement on multiple waveguides. This method allows the relative power change as a function of the waveguide length to be determined. By taking a log of the measured intensity, the slope of the corresponding fit line measures the attenuation of the structure per unit length ($y = mx + b$ where $m = 2k''$ [mm^{-1}] and $\alpha = 8.68k''$ [dB/mm]). The structure was measured for waveguide lengths of 6.76 mm and 3.26 mm, limited by the ability to obtain a successful cleave on sapphire. The error resulting from coupling and fabrication irregularities was 10%. The measured attenuation of our waveguides was 0.792 dB/mm, which corresponds to a propagation length of 5.48 mm. Again, this compares well with similar IMI structures using gold, which have achieved propagation lengths of 7 mm [13]. Simulations also were used to determine the propagation length of the structure which matches experimental results remarkably well, obtaining a propagation length of 5.68 mm for the same TiN structure. It is also important to note that the propagation length of the structure can be dramatically increased by reducing both the width and thickness of the TiN strip, at the expense of an expanded mode.

A summary of these results of the TiN structure, along with the competing structure on gold, are listed in Table 1. Due to the varying wavelengths of operation and metal thicknesses among published plasmonic waveguides, it was felt that additional structures could not be fairly compared to the results presented here.

With the material parameters, propagation length, and mode size determined, the FoMs can be evaluated for the two competing structures. As expected, gold has a larger FoM_1 than TiN due in large part to its significantly larger $|\mathrm{Re}\{\varepsilon\}|$. However, this also leads to a larger mode size for the gold structure. Typically the larger mode size would benefit gold enabling

#207666 - $15.00 USD Received 4 Mar 2014; revised 16 Apr 2014; accepted 6 May 2014; published 13 May 2014

lower propagation losses, but gold's intrinsic inability to form high quality thin films significantly affects its performance. Consequently, the epitaxial TiN structure obtains a similar propagation loss and a smaller mode size (larger FoM_2), despite having 'less ideal' material properties (smaller FoM_1). We note here that the gold waveguide was deposited on polymer layer that would normally increase the surface roughness. However, BCB was conceptualized by the semiconductor industry as a means to planarize layers for multilayer devices. Therefore, BCB typically has an extremely flat surface that is comparable to thermally grown SiO_2 (~2-3 Å rms) [44]. Consequently, we consider that BCB surface does not limit for the performance gold structure.

Table 1. Summary of Experimental Results for TiN Strip Waveguides on Sapphire Covered with Index Matching Oil*

Material	Metal Permittivity	Cladding Index	Strip Thickness [nm]	Strip Width [μm]	L_{prop} [mm]	α [dB/mm]	δ_z [μm]	FoM_1	FoM_2
TiN on Sapphire	−75 + 23i	1.75	10 nm	9.38	5.5	0.79	9.8	3	321
Gold on Polymer [13]	−132 + 13i	1.535	10 nm	8.0	7	0.6	20	10	229

*For comparison, the results from a similarly structured gold waveguide on a polymer are also shown. The FoM_1 = $Re\{\varepsilon\}/Im\{\varepsilon\}$ and $FoM_2 = L_{prop}/n\delta_z$ values for both waveguides are also shown. Gold has a higher FoM_1 than TiN mainly due to its significantly larger $|Re\{\varepsilon\}|$. However, when realistic devices are fabricated, the TiN device obtains a larger FoM_2.

4. Simulated structure using Si_3N_4 cladding

For practical devices, a solid-state structure is highly preferred. To provide the proper index match with the sapphire substrate and replace the index oil, a thin layer of silicon nitride is considered. By properly controlling the thickness the silicon nitride layer (n_{Si3N4} = 1.98 at 1.55 μm), the effective index of the silicon nitride plus the air in the superstrate can balance the sapphire substrate. However, this superstrate material should be carefully chosen. If the index of the superstrate is approximately the same as the substrate, for instance Si_xN_y (n ~1.76 at 1.55 μm), the required thickness to achieve plasmonic low-loss propagation will be quite large, roughly the scale of the mode size, which may not be practical for standard deposition methods. However, the propagation length would be weakly dependent upon the thickness of this superstrate, easing the tolerance during fabrication. Conversely, if the index of the superstrate is significantly larger than the substrate, for instance with silicon (n = 3.48 at 1.55 μm), the required thickness will be extremely small, and the propagation length will greatly depend upon the thickness of this layer. This would require extremely accurate deposition to achieve the desired condition.

In the subsequent analysis, a 9 μm wide TiN strip is considered for a thickness of 10 nm and 6 nm, and the height of the Si_3N_4 layer (h) is varied while recording both the propagation length and mode size of the resulting hybrid plasmonic mode, see Fig. 3 for a schematic. The permittivity of TiN is considered to be ε_{TiN} = −75 + 23i at 1.55 μm.

#207666 - $15.00 USD Received 4 Mar 2014; revised 16 Apr 2014; accepted 6 May 2014; published 13 May 2014

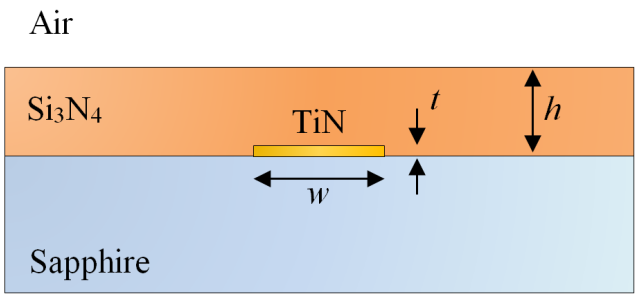

Fig. 3. Schematic of the solid-state waveguide system using a silicon nitride layer to obtain an effective index match with the sapphire substrate. The thickness (h) of the Si_3N_4 is varied and the propagation length and mode size are recorded. The width of the TiN strip is 9 μm and the thickness is considered to be 6 nm and 10 nm.

It is important to note that since the structure is not symmetric about the sapphire-Si_3N_4 interface, the LR-SPP mode should not be strictly introduced, as the resulting field profile will not be symmetric and entirely bound in the direction normal to the interface [5, 41]. For this structure, the resulting modes are called hybrid plasmonic-photonic modes. While these modes are even closer to photonic modes than the LR-SPP, the corresponding structures have been used to achieve a nice compromise between the modal confinement and propagation loss [45, 46]. Additionally, they retain many of the technological advantages of purely plasmonic structures such as better coupling to plasmonic devices and the ability to carry electrical and optical signals. However, it is noted that patterning of the Si_3N_4 layer could be used to form a photonic ridge waveguide. Nevertheless, the performance of this structure is critically dependent upon the sidewall quality, which can be a challenging fabrication problem. In this case, the plasmonic structure covered with a uniform Si_3N_4 layer would be more desirable because the ultra-thin TiN layer is easier and cheaper to etch, and would likely result in better sidewall quality.

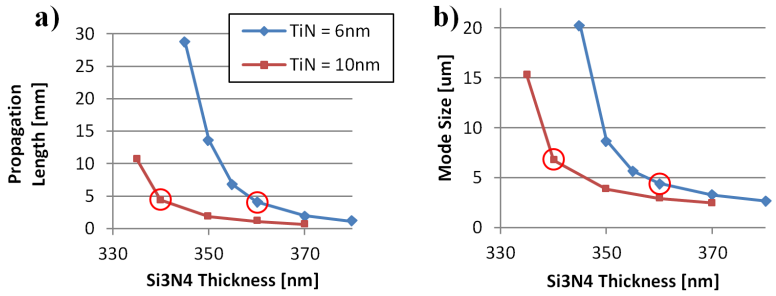

Fig. 4. a) Propagation length of the hybrid plasmonic mode versus the silicon nitride layer thickness. Modes for silicon nitride layers thinner than the cutoffs shown are predominately photonic in nature and are not considered. b) Mode size of the hybrid plasmonic mode versus the silicon nitride layer thickness. The highlighted data points illustrate that for a given propagation length, the thinner metal strip has a smaller mode size.

The propagation length of the hybrid plasmonic mode for a given silicon nitride height is shown in Fig. 4(a). For the Si_3N_4, the index contrast is such that the desired thickness is within reasonable bounds and the tolerance (a few nm's) is managable in practice. While modes exist for h below 345 nm (335 nm) for 6 nm (10 nm), respectively, these modes are predominately photonic in nature and are not considered in this analysis. The modal profile and z-cutline for the 6 nm thick TiN and 350 nm Si_3N_4 are shown in Fig. 5, achieving a mode size of 8.7 μm and a propagation length of 13 mm.

By considering the mode size for a given propagation length of the structure, an interesting trend is noted. Traditionally, the thought is that thinner metallic layers produce

#207666 - $15.00 USD Received 4 Mar 2014; revised 16 Apr 2014; accepted 6 May 2014; published 13 May 2014

larger mode sizes, which is generally true. However, if one considers designing the structure to achieve a specific propagation length, thinner metallic layers achieve the desired loss with a smaller overall mode size than thicker metallic layers (for example, consider L_{prop} = 5 mm, for t_{TiN} = 10 nm, t_{Si3N4} = 340 nm and δ_z = 6.5 µm, while for t_{TiN} = 6 nm, t_{Si3N4} = 360 nm and δ_z = 4 µm in Fig. 4 highlighted by red circles). This is somewhat in contrast to the typical thought process.

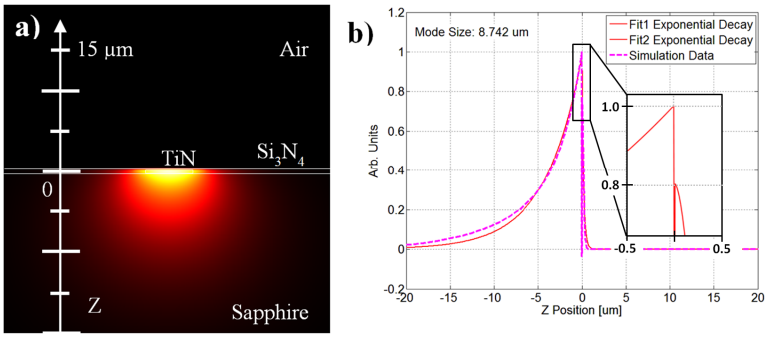

Fig. 5. a) Modal profile of the hybrid plasmonic mode for t = 6 nm, and h = 350 nm. b) z-cutline of the mode profile and curve fitting, illustrating a mode size of 8.7 µm. The inset is an enlarged view of the intensity distribution near the metal which illustrates the hybrid nature of the mode.

5. Conclusion

An LR-SPP plasmonic interconnect structure based on TiN was proposed and experimentally investigated at the telecommunication wavelength of 1.55 µm. The TiN strip waveguide was shown to obtain propagation lengths as high as 5.5 mm with a mode size of 9.8 µm, with the ability to reach greater than 10 mm given a more optimized geometry and solid-state cladding. The TiN waveguide was able to outperform similarly structured devices using gold, achieving a performance FoM_{2TiN} = 321 versus FoM_{2Au} = 229, despite having a smaller material metric, FoM_{1TiN} = 3 versus FoM_{1Au} = 10. This illustrates the importance of the epitaxial quality TiN film on c-sapphire for reducing the propagation losses. Structures which use a Si_3N_4 superstrate were also investigated theoretically, demonstrating propagation lengths of 13 mm with a mode size of 9 µm, or propagation lengths of 4 mm with a mode size of 4 µm for a 6 nm thick TiN layer. This work illustrates the importance of TiN as a realistic plasmonic material for future solid-state CMOS-compatible nano-optic devices, which maintain an equivalent performance level with competing plasmonic devices.

Acknowledgment

The authors would like to express their utmost appreciation to Dr. Sergey Bozhevolnyi and Dr. Ashwani Kumar from the University of Southern Denmark for their assistance in preliminary investigations. We acknowledge support from the following grants: ARO grant 57981-PHW911NF-11-1-0359), NSF MRSEC grant DMR-1120923 and NSF PREM DRM-0611430. M.F. wishes to acknowledge the Marie Curie Outgoing International Fellowship (contract no. 329346). V.E.B. acknowledges financial support from Otto Mønsteds and Kaj og Hermilla Ostenfeld foundations.